JOURNAL OF AIRCRAFT
Vol. 44, No. 1, January–February 2007

Tensile Stress Concentration Equation for Countersunk Holes

Kunigal N. Shivakumar* and Anil Bhargava†
North Carolina A&T State University, Greensboro, North Carolina 27411
and
James C. Newman Jr.‡
Mississippi State University, Mississippi State, Mississippi 39762

DOI: 10.2514/1.22900

A detailed three-dimensional finite element stress analysis was conducted for countersunk rivet and straight-shank holes in a plate subjected to tension loading. The study included a wide range of plate width to radius, thickness to radius, and countersunk depth to thickness ratios and countersunk angles (θ_c). The maximum stress concentration occurs at or near the countersunk edge. The stress concentration was found to be a function of countersunk depth, plate thickness and width, and it was nearly independent of the countersunk angle for $90 \leq \theta_c \leq 110$ deg. Using the finite element results and limiting conditions of countersunk hole configurations, an equation for stress concentration factor was developed and verified.

Nomenclature

b	=	depth of straight-shank portion of hole
C_s	=	countersink depth $(t - b)$
E	=	Young's modulus
h	=	one-half height of plate
K_t	=	maximum stress concentration factor along bore of hole under tension
$K_t(z)$	=	stress concentration factor along bore of hole under tension
r	=	radius of straight-shank portion of hole
S	=	applied remote tension stress
t	=	plate thickness
w	=	plate half-width
x, y, z	=	Cartesian coordinate system
θ_c	=	countersink angle
ν	=	Poisson's ratio

I. Introduction

RIVETING is a common method of joining structural components. Joining introduces discontinuities (stress risers) in the form of holes, change in load path, and additional secondary loads such as rivet bearing and bending. Because of these, local stresses at the joint are elevated compared to structural nominal stresses. Furthermore, wherever the aero/hydrodynamic surfaces are required, countersunk rivets are often used. Countersinking further complicates the stress flow and causes additional elevation of local stresses. These problems require a three-dimensional analysis. Accurate determination of these local stresses is essential to predict joint strength and fatigue life.

Exhaustive studies on stress concentration factor (SCF) in holes and notches for two-dimensional bodies subjected to a wide variety of loadings have been reported in the literature and these results are reported in handbooks [1,2]. Three-dimensional studies have also been made for plates with circular (straight-shank) holes subjected to remote tension [3–9]. Folias and Wang [6] provided a detailed review of previous analytical solutions and presented their series solution. The Folias and Wang solution covers a wide range of ratios of hole radius to plate thickness. A detailed 3-D finite element analysis (FEA) of straight-shank (SS) and countersunk hole specimens was made by Shivakumar and Newman [7,8] and their results are in agreement with Sternberg and Sadowsky [5] and Folias and Wang [6]. All these solutions were limited to wide plates. These studies resulted in the following conclusions:

1) Stress concentration is due to hoop stress along the bore of the hole.

2) Stress concentration depends on the dimensionless parameters t/r and z/t, where z is the thickness coordinate direction.

3) Stress concentration is highest in the midthickness of the plate for thin to moderately thick plates, but for thick plates, the stress concentration peaks near the free surface (at about $t/10$)

4) The state of stress is nearly plane-strain in the central region, is nearly plane-stress at the free surface, and is intermediate in the transition region. Thus, the stress flows into the central region of the plate, causing higher stress concentration than at the plate surface.

5) The stress concentration is about 4–7% higher than plane-stress value ($K_t = 3$) and it increases with plate thickness. Plane-stress value is recovered for very thin plates. The stress concentration is about 10% lower than plane-stress value at the free surface.

Only few papers have been published for countersunk rivet holes that directly relate to stress concentration. The first was by Wharley [9] in 1965 using birefringent coating on aluminum plates to measure the stresses on the surface of a plate with countersunk holes. Unfortunately, his experiment did not measure the stress concentrations at the edge of the countersink, where the concentration is highest. The other experimental work was by Cheng [10] in 1978 using stress freezing technique to obtain stress through the thickness of plate with a countersunk hole. He investigated a total of 13 configurations with different countersink angles and depths; seven specimens for tension loading and six for bending loading. Cheng's results showed conclusively that the highest stress concentration in the tension loading is at the edge of the countersink. In the early 1990s Shivakumar and Newman [7,8] conducted a detailed 3-D FE analysis of countersunk holes in a wide plate subjected to tension, bending, and wedge loadings. Their study included a wide range of countersink depth to thickness ratio, plate thickness to radius ratio, and countersink angle. Numerical results were presented in the form of charts and tables, along with a simple FORTRAN program including an interpolation method of determining K_t for any wide plate configuration. Their results did not include the width effect and lacked physical meaning of the

Received 1 February 2006; accepted for publication 9 October 2006.

*Director and Research Professor, Department of Mechanical and Chemical Engineering, Center for Composite Materials Research, Fort IRC. Associate Fellow AIAA

†Graduate Student, Department of Mechanical and Chemical Engineering, Center for Composite Materials Research, Fort IRC, Room 205.

‡Professor, Department of Aerospace Engineering, 314C Walker Engineering Building, P.O. Box A.

geometric parameters of the hole. In 1993, Young and Lee [11] conducted an independent 3-D FE analysis of plates with countersunk holes subjected to tension load. Their study included practical range of thickness, width, countersunk depth, and countersunk angle. Using the finite element results, Young and Lee came up with a design equation for stress concentration in countersunk holes. Young and Lee's solutions were based on a very coarse FE model; furthermore, their SCF equation did not reduce to 2-D solution in literature. Therefore, the present study is undertaken to establish accurate SCF for countersunk holes and then to develop a more accurate equation that satisfies the limiting conditions of the configurations. An exhaustive 3-D FE study with very fine modeling will be conducted. The parametric study includes countersunk angle, thickness to radius ratio, countersink depth to thickness ratio, and plate width to radius ratio. Based on these results and limiting solutions for straight-shank hole and thin plates, an equation for SCF in countersunk hole will be developed.

II. Rivet Hole Configurations

Figure 1 shows the configuration and nomenclature of a countersunk hole in a plate of height $2h$ and width $2w$, respectively, and subjected to a remote tensile stress σ_0. The hole radius was r and the depths of straight-shank and countersunk holes were b, C_s, respectively. The plate thickness was t, and b, C_s, and t are related by the equation $t = b + C_s$. The countersink angle was θ_c. By varying parameters C_s, t, and θ_c, one can simulate all cases of countersunk hole configurations from straight-shank ($C_s/t = 0$) to knife-edge ($C_s/t = 1$).

Plate thicknesses chosen in the study were $0.5r$, $1r$, $2r$, and $4r$ for all countersink configurations and an additional $0.4r$ and $10r$ were also included for straight-shank holes. Thickness cases $0.5r$–$2r$ represent aircraft structural joints and $2r$ and higher represent marine structures. Commonly used countersink angle in aircraft structures is 100 deg. The range of θ_c from 60 to 120 deg was chosen to evaluate the effect of countersink angle. The countersunk depths C_s chosen were 0 (straight-shank hole), $0.25t$, $0.5t$, $0.75t$, and $1.0t$. The case $C_s = t$ represents the knife-edge, which can occur due to poor control of drilling holes. First, a wide plate case was studied with half-width to radius ratio (w/r) of 15 and then finite width cases with $w = 2r$, $3r$, $4r$, $5r$, and $6r$ were studied to evaluate the width effect. The w/r of 2, 3, and 4 represent the practical cases in structural applications. In addition, some specific cases were also considered to verify the finite element model; those specific cases will be listed as and when they appear.

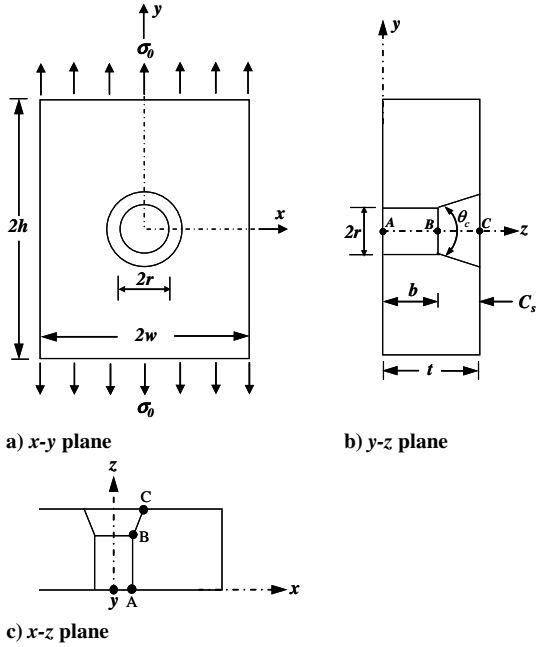

Fig. 1 Nomenclature, configuration, and loading of a countersunk rivet hole in a plate.

III. Definition of Stress Concentration Factor

Although the definition of the stress concentration factor is given in many classical books on theory of elasticity and in stress concentration handbooks, many of these solutions were for 2-D configurations. For 3-D configurations, the stress concentration varies along the bore of the hole. Therefore, the stress concentration is defined as a function of z-coordinate along the line formed by the intersection of $y = 0$ plane and the hole. The line connecting the points A, B, C in Fig. 1c defines the path of interest. Thus, $K_t(z)$ is the ratio of hoop stress σ_{yy} along the line A–B–C and the remote stress σ_0, $K_t(z) = \sigma_{yy}(z)/\sigma_0$. The stress concentration factor K_t is the maximum of $K_t(z)$.

IV. Finite Element Analysis

A three-dimensional finite element analysis was conducted using a commercial code ANSYS version 8.1 with the eight-noded hexahedron element SOLID45. The material property used was $E = 10e6$ and $\nu = 0.3$. Note that any finite value of E is acceptable because the SCF does not depend on E for isotropic plates. Because all configurations considered were symmetric about $x = 0$ and $y = 0$ planes, only one quarter of the geometry was modeled by imposing symmetry conditions on $x = 0$ and $y = 0$ planes and a restraining a node at $x = z = 0$ and $y = r$ against z-deformation. The FE idealization was made based on the concept that a finer mesh is used in the high-stress gradient regions and a coarser mesh in the low- or no-stress gradient regions. Typical FE mesh used for configurations $h/r = w/r = 5$ are shown in Figs. 2a and 2b, and for a narrow width plate is shown in Fig. 2c. Stress analysis was conducted for remote stress of $\sigma_0 = 1$, the resulting deformation and stress fields were examined, and the hoop stresses along the nodal line A–B–C were extracted. These stresses directly gave the stress concentration $K_t(z)$, because $\sigma_0 = 1$. An exhaustive comparison of present FE results, published data, and the mesh convergence study were made, and the results are presented in [12]. The present FE model results were within 1.4% of the finest model that had an element size (near the hole) of about 1/3 of the present model. Therefore, the present model is considered to be accurate. In the interest of the length of the paper only the important results are presented here.

V. Finite Element Results

As mentioned earlier, the FE analysis was conducted for a wide range of θ_c, C_s/t, t/r, and w/r values, keeping the loading as far as possible from the hole by selecting $h/r = 15$. These results are summarized first for a wide plate ($w/r = 15$) and then the results of finite width plate are presented.

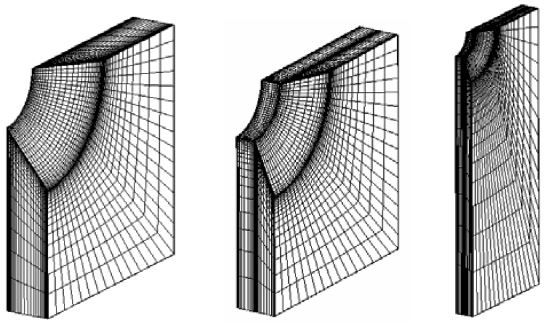

a) $h/r = w/r = 5$; $t/r = 1$; $C_s/t = 1$

b) $h/r = w/r = 5$; $t/r = 1$; $C_s/t = 0.5$

c) $h/r = 15$; $w/r = 6$; $t/r = 1$; $C_s/t = 0.5$

Fig. 2 Finite element models of three countersunk rivet hole configurations.

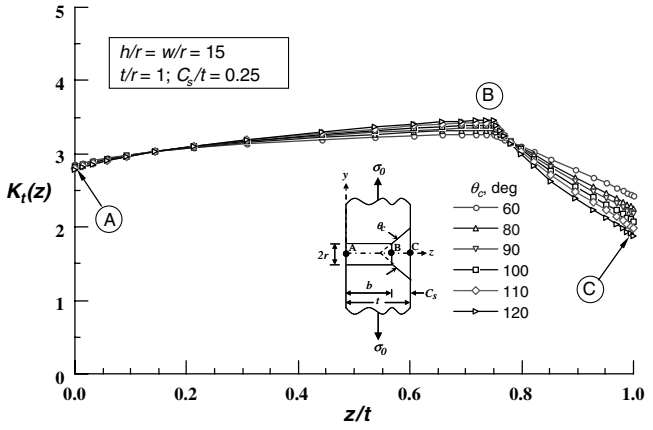

Fig. 3 Effect of countersink angle θ_c on $K_t(z)$ for a wide plate.

A. Effect of Countersink Angle

Figure 3 shows the variation of $K_t(z)$ along z/t for θ_c values ranging from 60 to 120 deg, including the results for $\theta_c = 100$ deg for $h/r = w/r = 15$, $t/r = 1$, and $C_s/t = 0.25$. The $K_t(z)$ is maximum at the countersink (B) and it decreases towards both the free edges. The $K_t(z)$ decreases much more rapidly towards the countersunk part (B–C) than towards the straight-shank part (B–A). The $K_t(z)$ at C is lower than that at A.

The stress concentration factor K_t increases with θ_c for the range of θ_c studied. This trend is in agreement with Shivakumar and Newman's [7,8] results, whereas it is opposite to that of Young and Lee's [11] results. The reason for the reversed trend in Young and Lee's analysis may be because of the coarseness of their FE model. The reason for the monotonic increase in K_t with θ_c, as observed here and in [7,8] is due to continuous channeling of load path towards and around the countersink edge. The K_t difference between $\theta_c = 90$ and 100 deg and between $\theta_c = 100$ and 110 deg is about 1%; therefore, the variation of K_t can be ignored for small deviations (± 10 deg) of θ_c from 100 deg, a practical angle used in the aircraft industry.

B. Effect of Countersink Depth (C_s/t)

The distribution of $K_t(z)$ along z/t for varying countersink depths is shown in Fig. 4 for $t/r = 1$. This distribution covers thin to thick plates. Results for other thicknesses are given in [12]. For thin plates ($t/r \leq 1$), K_t occurs at the countersink edge, whereas for thicker plates ($t/r \geq 2$), K_t occurs not at the countersink edge but slightly away from the edge (5% of t) and towards the SS portion of the hole. The K_t values generated for different values of C_s/t and t/r are listed in Table 1 and plotted in Fig. 5 (symbols). These results show that K_t increases monotonically with C_s/t until C_s/t is equal to about 0, and then decreases for all plate thicknesses less than $2r$ ($t/r < 2$).

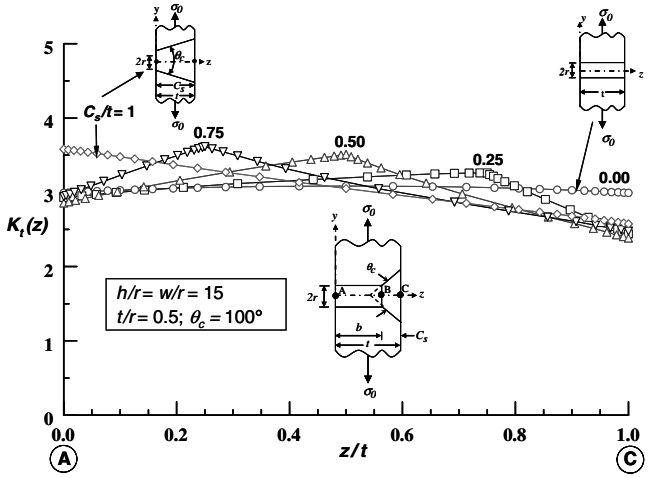

Fig. 4 Effect of countersunk depth on stress concentration distribution for a wide plate.

Table 1 Stress concentration $K_t(w/r = h/r = 15)$ from FEA

C_s/t	t/r							
	0.00	0.40	0.50	0.67	1.00	2.00	4.00	10.00
0.00	3.000	3.072	3.083	3.101	3.134	3.183	3.160	3.121
0.25	3.000	——	3.261	——	3.384	3.526	3.711	——
0.50	3.000	——	3.510	——	3.767	4.036	4.368	——
0.75	3.000	——	3.616	——	4.026	4.526	5.095	——
0.85	3.000	——	——	——	4.056	——	——	——
0.90	3.000	——	——	——	4.040	——	——	——
1.00	3.000	——	3.580	——	3.952	4.533	5.530	——

However, for thick plates, $t \geq 2r$, K_t continues to increase with C_s/t (including the knife-edge case). This trend was also noted by Shivakumar and Newman [7,8].

C. Effect of Thickness to Radius Ratio (t/r)

Figures 6 and 7 show the effect of t/r on $K_t(z)$ for $C_s/t = 0.5$ and 1. Values of $t/r = 0.5$, 1, and 2 represent the practical range of hole configurations used in aircraft industries and $t/r > 2$ is for thick structures: for example, marine industries. The K_t increases monotonically with t/r and it is consistent for all values of C_s/t; this can also be seen in Fig. 5. Based on the results presented in Figs. 4–7, it may be concluded that K_t is a coupled function of C_s/t and t/r.

D. Effect of Width to Radius Ratio (w/r)

The effect of plate width to hole radius ratio was studied by analyzing configurations of different C_s/t and w/r ratios. Figure 8 shows the $K_t(z)$ distribution for a SS hole ($C_s/t = 0$). The maximum value of $K_t(z)$ occurs in the central region and declines towards the

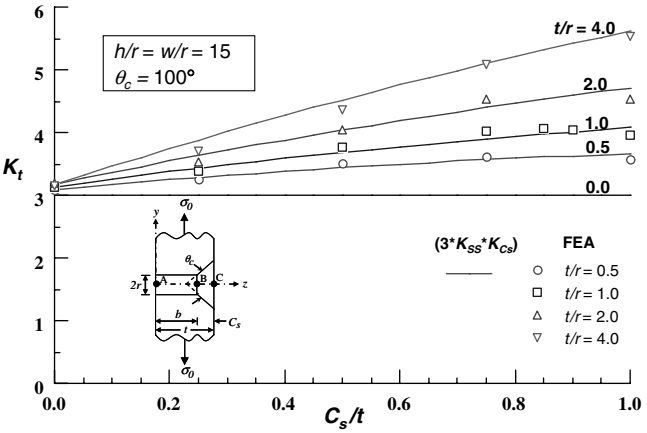

Fig. 5 FEA K_t results for various C_s/t and t/r configurations and also the K_t from an equation.

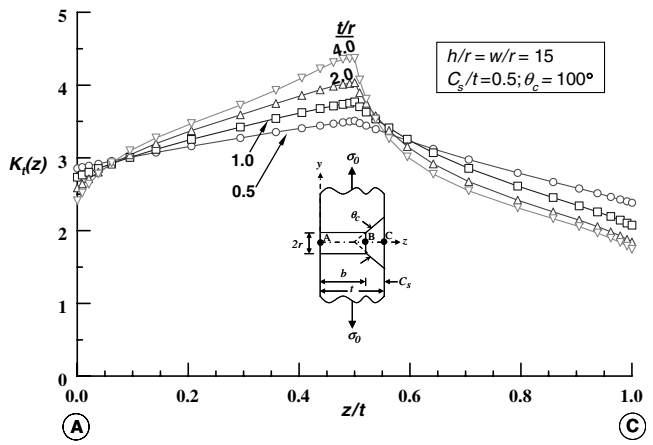

Fig. 6 Effect of t/r on stress concentration distribution for $C_s/t = 0.5$.

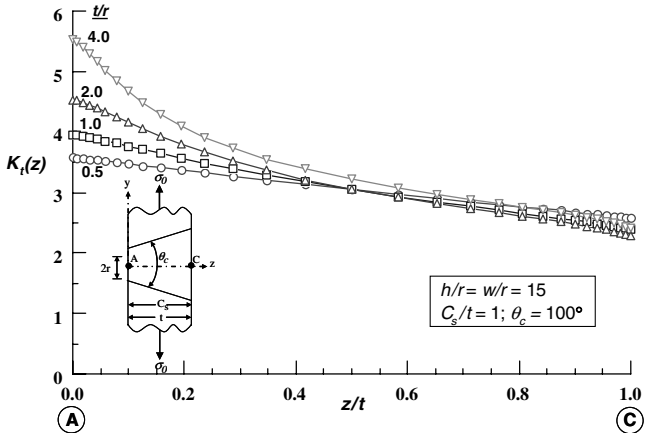

Fig. 7 Effect of t/r on stress concentration distribution for a knife-edge countersink.

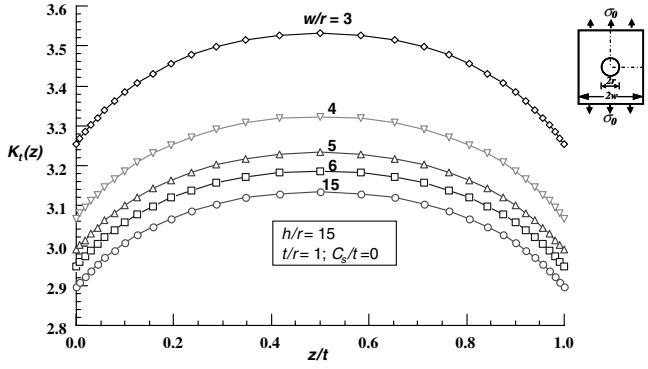

Fig. 8 Effect of w/r on stress concentration distribution (SS hole).

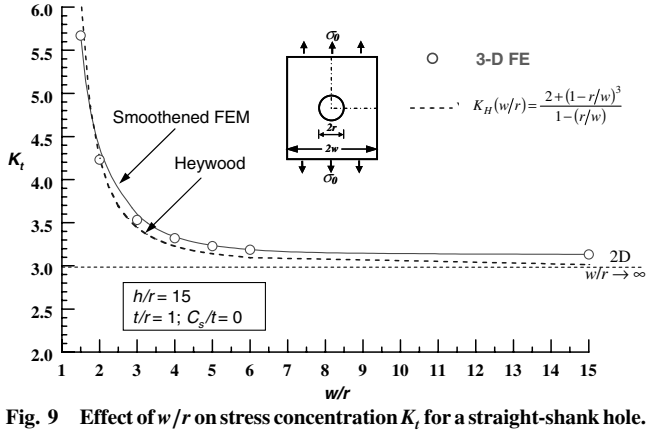

Fig. 9 Effect of w/r on stress concentration K_t for a straight-shank hole.

free surfaces. The free edge phenomenon, which is a result of the nonzero value of Poisson's ratio, has been very well explained by Sternberg and Sadowsky [5] for holes and by Shivakumar and Raju [13] for cracks in solids. The figure shows that $K_t(z)$ increases with decrease in w/r. The variation of K_t with w/r is shown in Fig. 9 for the SS hole configuration. In this case, K_t increases rapidly for $w/r < 3$ and it becomes infinity for $w/r = 1$, as expected. For $w/r > 6$, K_t is nearly constant, indicating that for wide plates K_t is independent of w/r. The plot also includes Heywood's [14] 2-D solution and the 2-D solution for an infinitely wide plate. The differences between the present FE and Heywood's equation is due to the 3-D effect. A close agreement between Heywood's solution with the 3-D FE results shows that an equation similar to Heywood equation could be used to approximate the width effect.

Figure 10 shows $K_t(z)$ distribution for different w/r ratios, for a countersunk hole of $C_s/t = 0.5$, $t/r = 1$, and $\theta_c = 100$ deg. As in

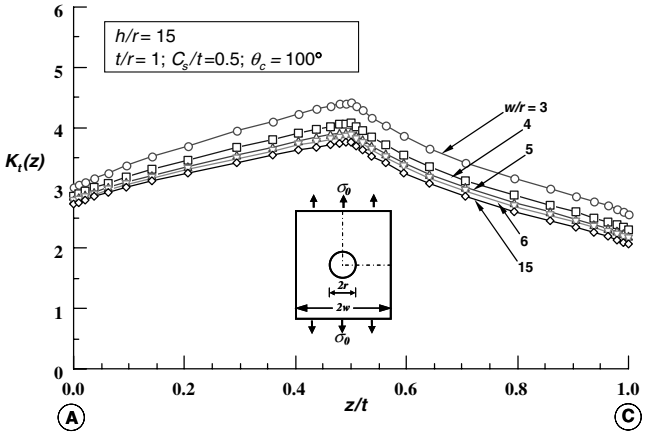

Fig. 10 Effect of w/r on stress concentration distribution ($C_s/t = 0.5$).

SS results, both $K_t(z)$ and K_t increase monotonically with decrease in w/r. The rate of increase in K_t rises as w/r falls below 4. The K_t results for different w/r and C_s/t values with $t/r = 1$ and $\theta_c = 100$ deg are listed in Table 2. These results will be used to verify K_t equation that will be developed later.

VI. 3-D Equation for Stress Concentration Factor (K_t)

Based on the FE results presented in the preceding section, an equation for K_t may be represented as a product of three functions, namely, $K_{SS}(t/r)$ for the SS hole, $K_{C_s}(C_s/t, t/r)$ for the countersunk holes and $K_H(w/r)$ for plate width effect. As previously mentioned, θ_c effect is ignored for small deviations (± 10 deg) of θ_c from $\theta_c = 100$ deg. Therefore, a general equation for K_t is written as

$$K_t = K_{SS}(t/r) \times K_{C_s}(C_s/t, t/r) \times K_H(w/r) \tag{1}$$

As previously mentioned, the finite width effect may be introduced through Heywood's 2-D stress concentration equation. The 2-D SCF varies from 3 to ∞ for $w/r = \infty$ to $w/r = 1$. Heywood's SCF equation is

$$K_H(w/r) = \frac{2 + (1 - r/w)^3}{1 - (r/w)} \tag{2}$$

This equation is further verified later by a separate 2-D FE analysis. Having selected K_H (w/r), the remaining two functions become a correction to K_H to account for 3-D and countersink geometry effects. The functions K_{SS} and K_{C_s} must vary from unity to a finite value depending on the hole geometry. The limiting conditions that K_{SS} and K_{C_s} functions have to satisfy are

1) SS hole ($C_s/t = 0$)

$K_{C_s} = 1$ and $K_{SS} = 1$ for plane-stress ($t/r \to 0$) and plane-strain ($t/r \to \infty$) conditions

2) Countersunk hole ($C_s/t \neq 0$)

$K_{SS} \neq 1$ and $K_{C_s} \neq 1$, in general, but for $t/r = 0$, $K_{SS} = 1$ and $K_{C_s} = 1$

Thus, K_{SS} and K_{C_s} will be determined by fitting equations to the FE results. The K_{SS} is obtained from SS data and K_{C_s} from countersink data. The FE results used for fitting the K_{SS} and K_{C_s} equations are listed in Table 1 and plotted in Fig. 5.

A. K_{SS} Equation Fit

The SS hole ($C_s/t = 0$) results in Table 1 were normalized by three (2-D SCF) and used to perform the K_{SS} equation fit. The form of the function is chosen such that it satisfies the limiting conditions that $K_{SS} = 1$ for $t/r \to 0$ (plane-stress) as well as $t/r \to \infty$ (plane-strain). The form of the equation chosen was

$$K_{SS}(t/r) = 1 + \frac{a(t/r)^{m_1}}{b + (t/r)^{m_2}} \tag{3}$$

Table 2 K_t results for finite width plates from FEA

C_s/t	w/r values						
	1.5	2	3	4	5	6	15
0.00	5.670	4.231	3.532	3.323	3.233	3.187	3.134
0.25	——	——	3.880	3.623	3.514	3.457	3.384
0.50	——	——	4.428	4.078	3.931	3.857	3.767
0.75	——	——	4.827	4.398	4.220	4.130	4.026
1.00	——	——	4.834	4.381	4.178	4.073	3.952

The four constants a, b, m_1, and m_2 were determined by the minimization of error between the equation and the FE results and then subsequently reducing of the constants to a simple form. Note that constants a, b, m_1, and m_2 are temporary variables chosen only for the curve fit and they do not have any meaning beyond this section. The determined K_{SS} equation is

$$K_{SS}(t/r) = 1 + \frac{0.5(t/r)^{0.6}}{10 + (t/r)^{1.6}} \tag{4}$$

A comparison of the equation with the SS hole FE results is shown in Fig. 11. The K_{SS} equation agrees within 0.5% of the FE results. The correlation factor of the fit is greater than 0.98.

B. K_{C_s} $(C_s/t, t/r)$ Equation Fit

The countersink hole K_t results in Table 1 were normalized by SS $(C_s/t = 0)$ data and these results were used to perform a multiparameter (t/r and C_s/t) fit to obtain the K_{C_s} equation. A simple quadrating polynomial in C_s/t multiplied by the t/r power function was chosen.

$$K_{C_s}\left(\frac{C_s}{t}, \frac{t}{r}\right) = 1 + a_1\left(\frac{C_s}{t}\right)\left(\frac{t}{r}\right)^{b_1} - a_2\left(\frac{C_s}{t}\right)^2\left(\frac{t}{r}\right)^{b_2} \tag{5}$$

Through a multiparameter fit, the constants a_1, a_2, b_1, and b_2 were determined. These constants were further simplified to arrive at simple numbers. The resulting equation is

$$K_{C_s}\left(\frac{C_s}{t}, \frac{t}{r}\right) = 1 + 0.4\left(\frac{C_s}{t}\right)\left(\frac{t}{r}\right)^{0.6} - 0.1\left(\frac{C_s}{t}\right)^2\left(\frac{t}{r}\right)^{0.3} \tag{6}$$

Figure 5 shows a comparison of the equation $K_t = 3 \times K_{SS} \times K_{C_s}$ with the FE data in Table 1 for different values of C_s/t and t/r. The solid lines represent the equation and the symbols represent the FE data. Maximum difference between the equation and the FE data is approximately 3% and the correlation factor of the equation with the FE data is greater than 0.99. Thus, the K_{C_s} equation is sufficiently accurate to account for the countersunk depth and plate thickness to hole radius ratios.

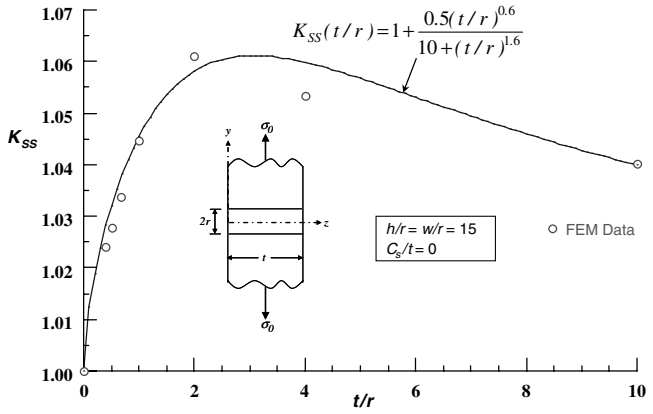

Fig. 11 3-D stress concentration factor for a straight-shank hole (wide plate).

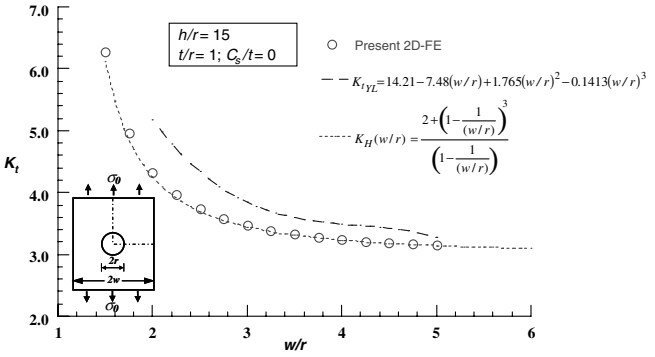

Fig. 12 Comparison of stress concentration factor for finite width plate from different analyses (2-D).

C. Finite Width Panel, $K_H(w/r)$

Although Heywood's [14] width correction equation, $K_H(w/r)$, was chosen in the K_t Eq. (1), the accuracy of the Heywood equation, which was also empirical, was verified by separate 2-D FEA. A separate 2-D FE model was made using the same modeling strategy and the mesh refinement as in the 3-D model. The stress analysis was conducted for different w/r values varying from 1.5 to 6 and the K_t results were extracted.

The K_t values obtained by 2-D FEA and Heywood's Eq. (2) are compared in Fig. 12 along with Young and Lee's 2-D design equation [11]. The FE results and Heywood's K_H equation agreed within 1% of each other except for a very narrow plate $w/r = 1.5$. The difference for this case is 2.7%. Young and Lee's [11] equation, which is valid for $2 \le w/r \le 5$, overestimated K_t by more than 10% for all values of w/r considered. The difference is larger for smaller w/r. Thus, Heywood's equation is accurate and simple to approximate the w/r effect.

Finally, the K_t equation for the countersunk rivet hole in a plate subjected to remote tensile stress becomes Eq. (1), and the functions K_H, K_{SS}, and K_{C_s} are given by Eqs. (2), (4), and (6), respectively.

For a wide plate, Eq. (1) simplifies to

$$K_t = K_{SS}(t/r) \times K_{C_s}(C_s/t, t/r) \tag{7}$$

The preceding equation is valid for $90 \le \theta_c \le 110$ deg.

VII. Verification of K_t Equation

A. Comparison with FE Results

The K_t Eq. (1) is verified by comparing it with the FE results used in fitting the equation and by the new data generated for this purpose. The comparisons are made first for the wide plate ($w/r = 15$) and then for finite width plates.

Figure 13 shows the comparison of the FE results and Eq. (1) for different C_s/t and t/r values. The percent difference between the

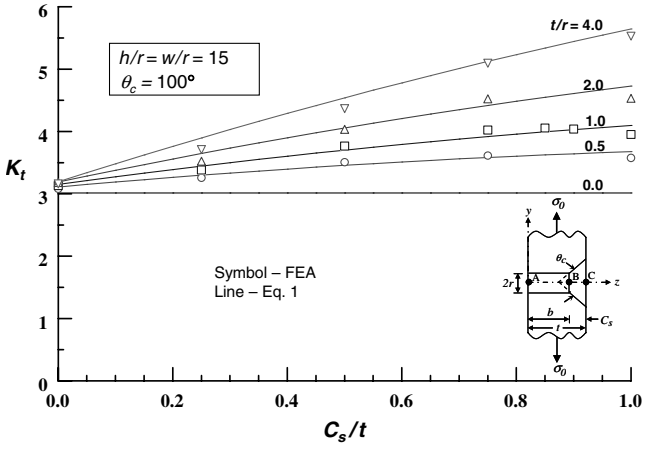

Fig. 13 Comparison of K_t Eq. (1) with FEA for wide plate.

Table 3 Percent difference between Eq. (1) and FEA for wide plates

C_s/t	Percent Difference $= [(K_{t_{eq.}} - K_{t_{FEA}})/K_{t_{FEA}}] \times 100$							
	t/r							
	0.00	0.40	0.50	0.67	1.00	2.00	4.00	10.00
0.00	0.5	0.9	0.9	0.8	0.5	0.2	1.1	0.4
0.25	0.5	——	1.2	——	1.8	3.5	5.0	——
0.50	0.5	——	−1.5	——	−1.7	0.6	4.0	——
0.75	0.5	——	−0.9	——	−2.6	−2.4	0.6	——
0.85	0.5	——	——	——	−1.5	——	——	——
0.90	0.5	——	——	——	−0.3	——	——	——
1.00	0.5	——	2.8	——	3.7	4.3	2.1	——

two results is summarized in Table 3. The maximum error in the equation is 5% or less for all the cases analyzed.

Figure 14 shows a comparison between the FE results and Eq. (1) for finite width plates; the percent difference between the two are summarized in Table 4. Only one typical case of t/r is presented. The maximum difference between the Eq. (1) and FEA is less than or equal to 5% for most cases, except for $C_s/t = 0.75$ and $w/r = 3$, where the error is about 7%. The error increases for very narrow width plates (for example, $w/r = 1.5$), which is not a practical configuration.

B. Comparison with Young and Lee's Design Equation

Young and Lee [11] proposed a design equation based on their FE analyses and British Aerospace's 2-D experimental design equation to account for the width effect. The K_t equation is represented as and is given by

$$K_{t_{YL}} = [K_{C_s}(C_s/t)]_{YL} \times [K_w(w/r)]_{YL} \tag{8}$$

where

$$[K_{C_s}(C_s/t)]_{YL} = 0.959 + 0.673(C_s/t)$$

$$[K_w(w/r)]_{YL} = 14.21 - 7.48(w/r) + 1.765(w/r)^2 - 0.1413(w/r)^3$$

Note that $K_{t_{YL}}$ is not a function of t/r. The equation was intended for aircraft joint configurations. Figure 15 shows a comparison of the present K_t Eq. (1) with Young and Lee's $K_{t_{YL}}$ Eq. (8) for $t/r = 0.5$. The two K_t equations differed widely and this difference may be as small as "zero" to as large as 55%. Because the present K_t equation is based on refined and accurate FE model, it is believed to be accurate, and Young and Lee's equation is overly conservative.

In summary, the stress concentration Eq. (1) is general, accurate, and satisfies all limiting cases. The equation is valid for straight-shank, countersunk including knife-edge holes, and for a wide range of plate sizes.

Table 4 Percent difference between Eq. (1) and FEA for finite wide plates

C_s/t	Percent Difference $= [(K_{t_{eq.}} - K_{t_{FEA}})/K_{t_{FEA}}] \times 100$						
	w/r						
	1.5	2	3	4	5	6	15
0.00	12.7	5.0	2.0	1.6	1.5	1.5	0.5
0.25	——	——	1.5	1.9	2.2	2.3	1.8
0.50	——	——	−4.4	−2.7	−1.9	−1.4	−1.7
0.75	——	——	−7.2	−4.5	−3.2	−2.6	−2.6
1.00	——	——	−3.2	0.2	2.2	3.3	3.7
0.90	0.5	——	——	——	−0.3	——	——
1.00	0.5	——	2.8	——	3.7	4.3	2.1

VIII. Conclusions

A detailed three-dimensional finite element stress analysis was conducted on straight-shank and countersunk rivet holes in a plate subjected to tension loading. The study included a wide range of plate widths, thicknesses, countersunk depths, and countersunk angles. Results confirmed the previous result that the stress concentration is maximum at the countersink for thin and moderately thick plates and it occurs near (about $0.05t$) the countersink and on the straight-shank part of the hole for thick plates with shallow countersinks. The maximum value of the stress concentration is referred to as the stress concentration factor K_t. The K_t depends on the countersunk depth, plate thickness, and width to radius ratios. The K_t variation for a practical range of countersunk angles (90–110 deg) is small (about 1%) and therefore its effect can be neglected. Using the finite element K_t results and limiting conditions, an equation for K_t was developed. The expression for K_t for $90 \leq \theta_c \leq 110$ deg is given by

$$K_t = K_{pl}(t/r) \times K_{C_s}(C_s/t, t/r) \times K_H(w/r)$$

where

$$K_{pl}(t/r) = 1 + \frac{0.5(t/r)^{0.6}}{10 + (t/r)^{1.6}}$$

$$K_{C_s}\left(\frac{C_s}{t}, \frac{t}{r}\right) = 1 + 0.4\left(\frac{C_s}{t}\right)\left(\frac{t}{r}\right)^{0.6} - 0.1\left(\frac{C_s}{t}\right)^2\left(\frac{t}{r}\right)^{0.3}$$

$$K_H(w/r) = \frac{2 + (1 - r/w)^3}{1 - (r/w)}$$

This equation is accurate within 5% of finite element data for a wide range of widths, countersunk depths, and plate thicknesses. The maximum error is about 7% for $w/r = 3$, $t/r = 1$, and $C_s/t = 0.75$, but less than 5% for all other cases. Young and Lee's [11] design equation differed from the present K_t equation. The difference varied

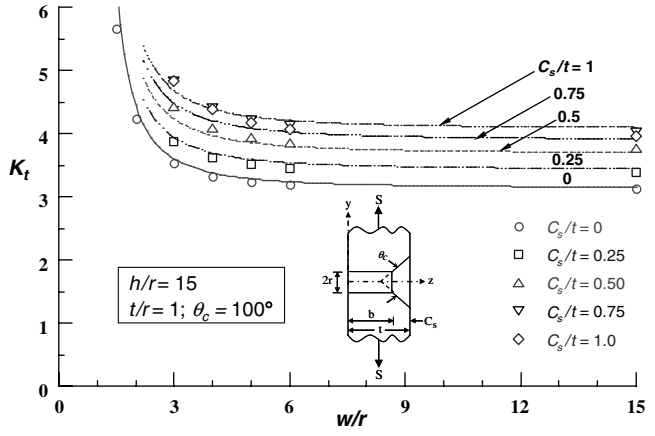

Fig. 14 Comparison of K_t Eq. (1) with FEA for finite width plates ($t/r = 1$; $h/r = 15$).

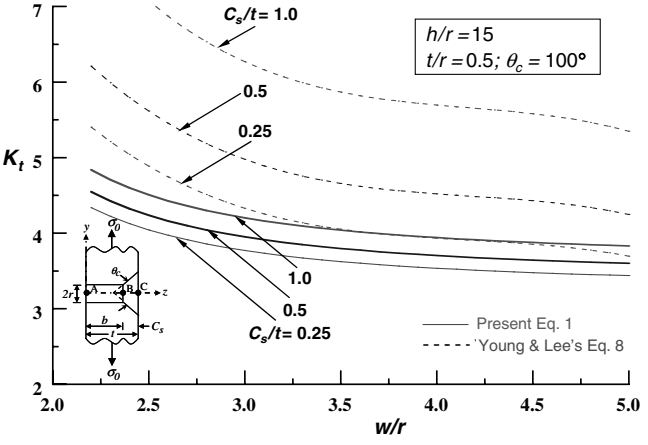

Fig. 15 Comparison of present and Young and Lee's K_t equation results as a function of w/r ($t/r = 1$).

from as small as zero, to as large as 55%. In summary, the stress concentration equation presented in this paper is general, accurate, and satisfies all limiting cases. The equation is valid for a wide range of countersunk hole configurations, including the knife-edge, and plate widths.

Acknowledgments

The authors wish to thank Yapa Rajapakse and the Office of Naval Research through the grant no. N 00014-01-1033 and the Federal Aviation Administration subcontract (through Iowa State) through the contract no. DTFA03-98-D-0008 for their support.

References

[1] Pilkey, W. D., *Peterson's Stress Concentration Factors*, 2nd ed., John Wiley & Sons, New York, 1997.

[2] Savin, G. N., *Stress Concentration Around Holes*, Pergamon, New York, 1961.

[3] Green, A. E., "Three-Dimensional Stress Systems in Isotropic Plates, Part 1," *Philosophical Transactions. Series A, Mathematical, Physical, and Engineering Sciences*, Vol. 240, April 1948, pp. 561–597.

[4] Neuber, H., *Theory of Notch Stresses: Principles for Exact Stress Calculation*, J. W. Edwards, Ann Arbor, MI, 1946.

[5] Sternberg, E., and Sadowsky, M. A., "Three-Dimensional Solution for the Stress Concentration Around a Circular Hole in a Plate of Arbitrary Thickness," *Journal of Applied Mechanics*, Vol. 16, No. 1, 1949, pp. 27–38.

[6] Folias, E. S., and Wang, J. J., "On the Three-Dimensional Stress Field Around a Circular Hole in a Plate of Arbitrary Thickness," *Computational Mechanics*, Vol. 6, No. 3, 1990, pp. 379–391.

[7] Shivakumar, K. N., and Newman, J. C., Jr., "Three-Dimensional Stress Concentration Factor in Straight-Shank and Countersunk Rivet Holes in Plates Subjected to Various Loading Conditions," NASA TP 3192, 1992.

[8] Shivakumar, K. N., and Newman, J. C., Jr., "Three-Dimensional Stress Concentration Equations for Straight-Shank and Countersunk Rivet Holes in Plates Subjected to Various Loading Conditions," *Journal of Applied Mechanics*, Vol. 62, March 1995, pp. 248–249.

[9] Wharley, R. E., "Stress-Concentration Factors for Countersunk Holes," *Experimental Mechanics*, Vol. 5, No. 8, 1965, pp. 257–261.

[10] Cheng, Y. F., "Stress-Concentration Factors for a Countersunk Hole in a Flat Bar in Tension and Transverse Bending," *Journal of Applied Mechanics*, Vol. 45, No. 4, 1978, pp. 929–932.

[11] Young, J. B., and Lee, K. K., "Stress Concentration Factors in Countersunk Holes,"*The Aeronautical Journal*, Vol. 968, Oct. 1993, pp. 267–276.

[12] Bhargava, A., "Three-Dimensional Tensile Stress and Strain Concentration Equations for a Countersunk Hole," Ph.D. Dissertation, North Carolina Agricultural and Technical State Univ., Greensboro, NC, 2006.

[13] Shivakumar, K. N., and Raju, I. S., "Treatment of Singularities in Cracked Bodies," *International Journal of Fracture*, Vol. 45, No. 3, 1990, pp. 159–178.

[14] Heywood, R. B., *Designing by Photoelasticity*, Chapman and Hall, London, 1952.